Functionality-Induced Locking of Zeolitic Imidazolate Frameworks

Tongtong Xu, Beibei Zhou, Yu Tao, Zhaolin Shi, Wentao Jiang, Mahmoud Abdellatief, Kyle E. Cordova, and Yue-Biao Zhang*

ACCESS | Metrics & More | Article Recommendations | Supporting Information

ABSTRACT: Zeolitic imidazolate frameworks (ZIFs) are metal—organic analogues of zeolites that have attracted considerable interest for gas separation applications. However, the inherent framework flexibility of ZIFs during gas adsorption complicates their designed and desired performance. Herein, we report functionality-induced locking of ZIFs undergoing irreversible structural transformations, which leads to exceptional framework rigidity. Specifically, an isoreticular series of zeolite GME-type Co^{II}-ZIFs were prepared and proven to have dynamic, flexible, and rigid behaviors after thermal activation, depending on their functional groups (i.e., $-H$, $-CH_3$, and $-NO_2$). Molecular insights into the irreversible, functionality-induced locking were determined to occur as a consequence of framework flexibility for maximizing the linker—linker interactions from $\pi-\pi$ interaction to hydrogen bonding. The practical impact of functionality-induced locking in ZIFs was evaluated through high-pressure CO_2/CH_4 adsorptive separation for realizing more efficient methane purification. The present findings shed light on the deliberate control over the inherent flexibility observed in many porous materials to optimize their performance in practical applications.
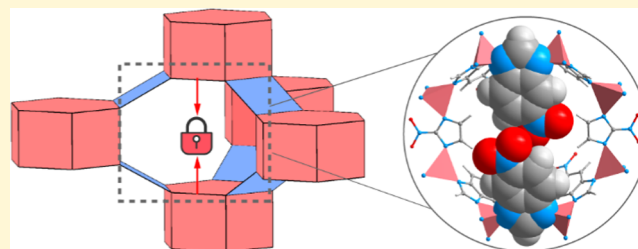
1. INTRODUCTION

As a subclass of metal—organic frameworks (MOFs),[1,2] zeolitic imidazolate frameworks (ZIFs) are constructed by stitching tetrahedral metal centers (M = Co^{II}, Zn^{II}, Cd^{II}, and Li^{I}/B^{III}, among others)[3–7] together using imidazolate and its functionalized derivatives to form tetrahedral networks resembling those structural types observed or even unrealized in inorganic zeolites.[8–12] Featuring exceptional chemical stabilities and accessible microporosity, ZIFs have attracted considerable attention for use in carbon capture and industrial gas separations, given their pronounced architectural rigidity and ease of functionalization.[13–15] However, the imidazolate linkers used to construct ZIFs are usually dynamic via swinging motions, which imposes inherent framework flexibility during gas adsorption.[16–26] This phenomenon directly impacts ZIFs' performance in practical gas separation processes, especially at higher gas pressures. Ingenious strategies have been proposed in membrane separation processes to suppress the swinging motion of linkers by introducing external stimuli that lead to enhanced separation performance,[27–30] but such strategies remain underdeveloped in the practice of adsorptive gas separation processes, such as pressure swing adsorption (PSA). Therefore, we sought to develop a new reticular chemistry principle to control the intrinsic linker dynamics of ZIFs through molecular design.[31–33]

Secondary building units (SBUs), such as 3-ring (3R),[34–37] double 4-ring (D4R),[38,39] and double 6-ring (D6R),[13,40–42] are critical structural motifs to realize topological designability and architectural rigidity in ZIFs.[43] Herein, we report a strategy

that harnesses the structural transformation and functionality-induced locking of the D6Rs in zeolite GEM-type ZIFs to enhance the overall framework rigidity further (Scheme 1a). Inspiration for selecting a flexible network was based on the fact that the **acs-a** net observed in MOFs exhibits a large amplitude of structural transformation upon guest inclusion and removal.[44–46] Given that the GME net can be regarded as a geometric variation of the **acs-a** net through edge decoration, we targeted the design, synthesis, and characterization of the GME-type isoreticular series of Co^{II}-based ZIFs with various functional groups (i.e., $-H$, $-CH_3$ and $-NO_2$) on the benzimidazolate linkers (Scheme 1b). These ZIFs are all constructed from Co^{II} tetrahedral centers and 2-nitro-imidazolate (nIm) mixed with benzimidazolate (bIM; ZIF-68-Co), 5-nitrobenzimidazolate (nbIM; ZIF-78-Co), or 5-methylbenzimidazolate (mbIM; ZIF-79-Co) in a 1:1 linker molar ratio. The porous structures comprise one type of channel (*t-kno*) and two types of cages (Cage A, *t-hpr*; cage B, *t-gme*; Scheme 1c) in a 1:1:1 ratio, with the respective functional group dangling in the pores.

Swinging motions of imidazolate linkers have been observed in ZIFs as a dynamic phenomenon during gas adsorption for

Scheme 1. Design Principle for Achieving Intermolecular, Functionality-Induced Locking in ZIFs (a) Geometric Variation from the acs-a to the GME Net When Considering the Double 6-Rings as Rigid Joints and the Bridging 4-Rings as Flexible Hinges. (b) Linking Co^{II} Tetrahedral Centers with 2-Nitroimidazolate (nIm) and Different Functionalized Benzimidazolates (RbIM) Produced an Isoreticular Series of GME-ZIFs. (c) Single-Crystal Structure of ZIF-78-Co
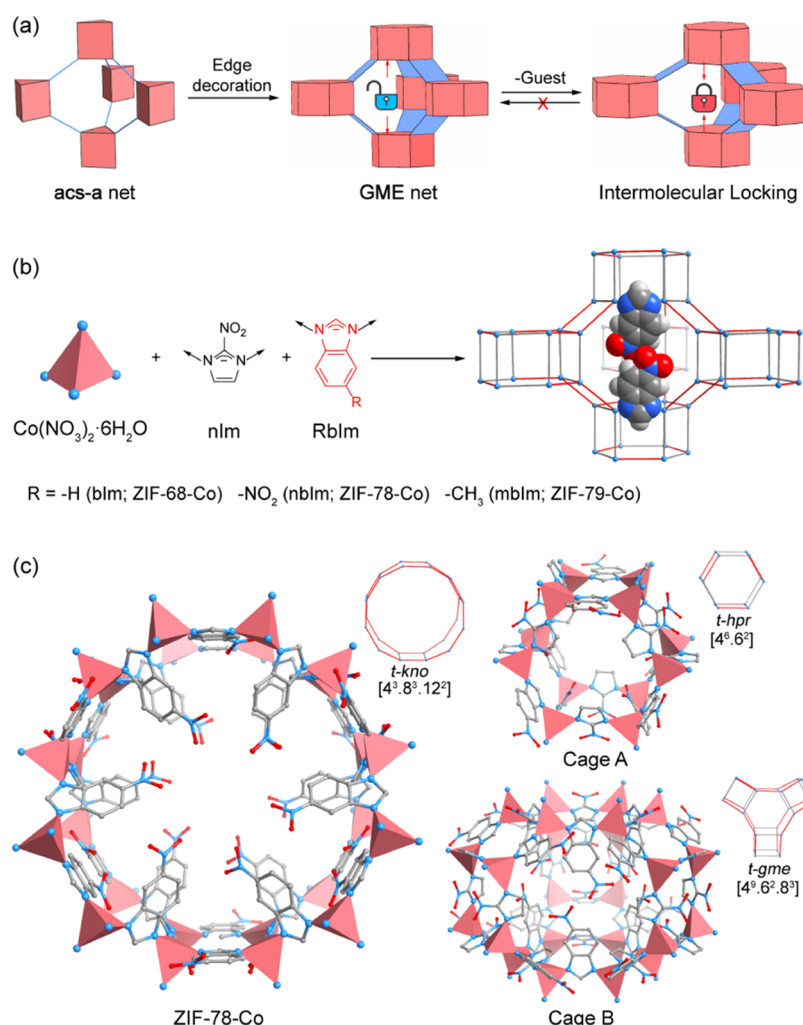
extra gas uptake. This is best exemplified by the zeolite SOD-type ZIF-8.[16−19] Although significant structural transformation due to this linker swinging motion has rarely been investigated, recently, reversible structure transformation was studied during guest removal and adaptive inclusion of guest molecules in zeolite SOD ZIF-65, which exhibited a large amplitude of distortion in its SOD cages.[20,21] Herein, we uncover functionality-induced locking in ZIFs that leads to an irreversible structural transformation, highlighted by a significant contraction of their unit cells upon thermal activation to rigidify the framework. This finding conceptually advances the importance of functionality-induced locking via framework flexibility by a maximal linker−linker interaction. Interestingly, such hidden phenomena have been overlooked in many porous materials, especially for MOFs and COFs,[47−51] yet it is essential for elucidating their anomalous adsorption behavior and understanding the energy landscape of the framework. In this contribution, we harness a flexible network and the ease of imidazolate linker functionalization to lock the framework into a global energy minimum with a significant energy barrier for reversible structure transformation. Finally, we detail the importance of this strategy for improving the

utility of ZIFs and enabling their practical application in adsorptive gas separation using PSA for methane purification.

2. EXPERIMENTAL SECTION

2.1. Preparation and Characterization of ZIF Materials. Two new ZIFs, namely, ZIF-78-Co [Co(nIm)(nbIm)] and ZIF-79-Co [Co(nIm)(mbIm)], and a reported one, ZIF-68-Co [Co(nIm)-(bIm)],[52] were prepared through solvothermal reactions of Co-(NO$_3$)$_2$·6H$_2$O with nIm and RbIm (R = −H, −CH$_3$, −NO$_2$) in *N*,*N*-dimethylformamide (DMF) at 85 °C for 7 days, yielding violet hexagonal prismatic crystals. The as-synthesized samples were washed and refreshed with ethanol (EtOH) for 2 weeks, followed by degassing under vacuum at 200 °C for 8 h.

The crystal morphologies of the as-synthesized samples were examined using a scanning electron microscope (Phenom-World BV, ProX; Figure S1.1 in Supporting Information, SI). Thermogravimetric analyses (TGA) of the activated samples were performed on a TGA instrument (PerkinElmer, TGA 4000) with a heating rate of 5 °C/min from ambient temperature to 700 °C under N$_2$ flow, which demonstrated high thermal stability (300 °C) and the complete removal of guest molecules for all members (Figure S1.2 in SI). Elemental analyses were performed on an elemental analyzer (PerkinElmer, SERIES II 2400). The formulae of the activated ZIFs were confirmed by their digested-solution ^{1}H nuclear magnetic
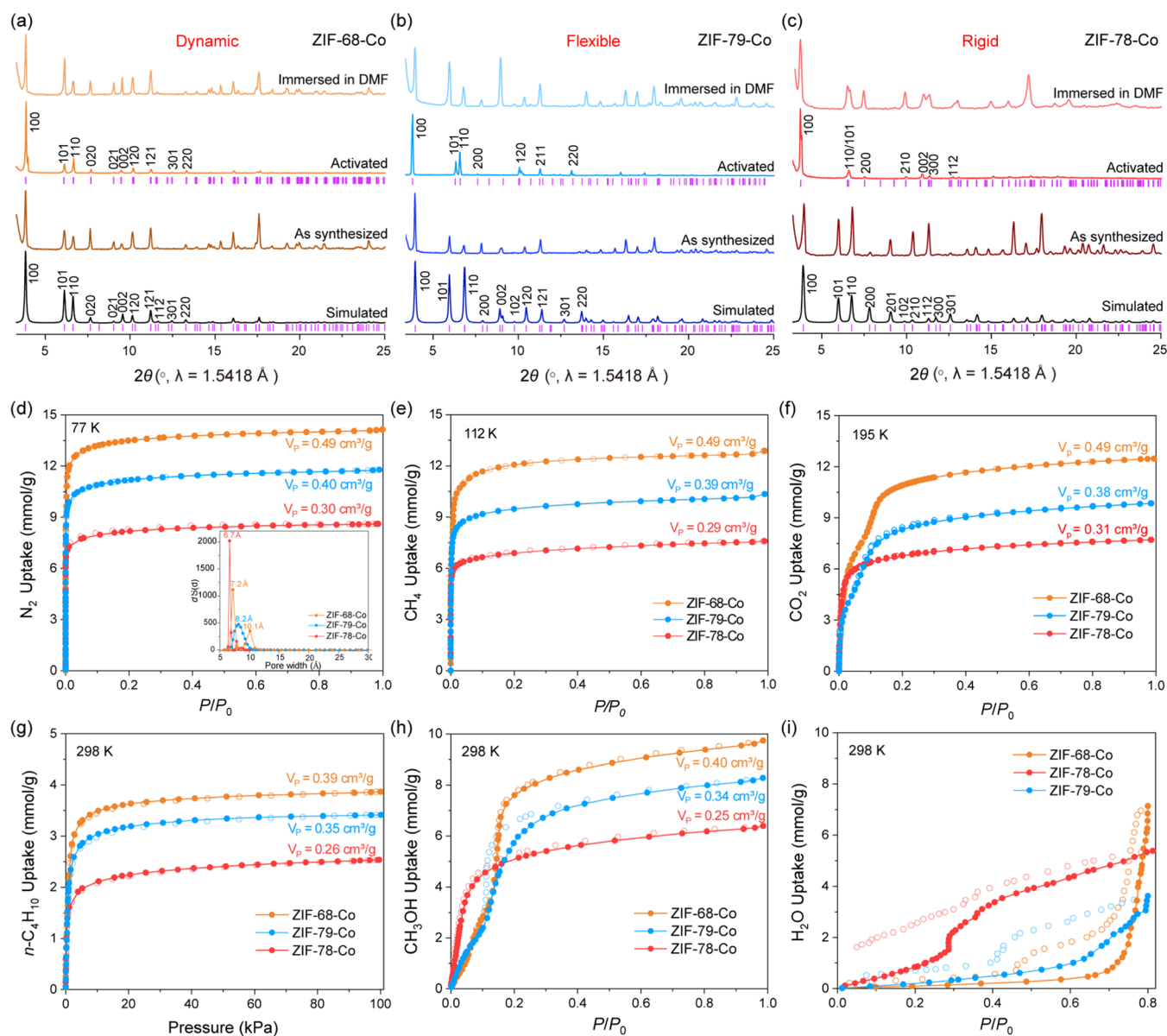
Figure 1. Dynamic behaviors of the GME-ZIFs as revealed by as-synthesized/activated PXRD patterns and gas/vapor adsorption isotherms. (a) Indexed PXRD marks of ZIF-68-Co displayed unchanged unit cell parameters. Indexed PXRD patterns of ZIF-79-Co (b) and ZIF-78-Co (c) exhibited significant changes to their unit cell parameters. Gas adsorption isotherms for ZIF-68-Co (orange), ZIF-79-Co (blue), and ZIF-78-Co (red) for (d) N_2 at 77 K; (e) CH_4 at 112 K; (f) CO_2 at 195 K, and (g) n-C_4H_{10} at 298 K demonstrated that ZIF-78-Co was more rigid than ZIF-68-Co and ZIF-79-Co. Vapor adsorption isotherms for ZIF-68-Co, ZIF-79-Co, and ZIF-78-Co for (h) methanol (CH_3OH) at 298 K demonstrated that the three GME-ZIFs exhibited different dynamic behaviors and (i) H_2O at 298 K showed that ZIF-68-Co and ZIF-79-Co were hydrophobic, whereas ZIF-78-Co was relatively hydrophilic.

resonance (NMR) spectra, which were collected on a Bruker AVANCE NEO 400 (400 MHz) NMR spectrometer, with deuterated dimethyl sulfoxide as the solvent (Figures S1.3−S1.5 in SI). Infrared spectra were collected on an FT-IR spectrometer (PerkinElmer, Frontier), which indicated the exact composition of the as-synthesized and activated samples and full activation with no solvent molecules present (Figures S1.6−S1.8 in SI).

2.2. X-ray Diffraction. Single-crystal X-ray diffraction (SCXRD) data of the as-synthesized and activated ZIFs were collected on a Bruker D8 Venture Photon III diffractometer using a Ga Kα X-ray source or collected at BL17B (λ = 0.6701 Å) and BL10U2 (λ = 0.6887 Å) stations of Shanghai synchrotron radiation facility. The activated samples were sealed in 0.3-mm (I.D.) capillaries under an argon atmosphere in a glovebox equipped with an optical microscope (Section S2 in SI).

Powder X-ray diffraction (PXRD) patterns of solvated samples were recorded on a Bruker D8 Advance diffractometer with Cu Kα radiation (λ = 1.5418 Å). Data were collected in the 2θ range of 3− 25° with a step size of 0.02°. Temperature-dependent PXRD data were collected at the BL14B1 beamline at the Shanghai synchrotron radiation facility (λ = 0.6895 Å, 2θ range of 1−30°) or the MS beamline at the SESAME synchrotron (λ = 0.8270 Å, 2θ range of 1- 50°). Guest-free samples were sealed in a 0.8 or 0.5 mm inner diameter (I.D.) capillary. Temperature-dependent synchrotron PXRD measurements also proved the thermal stability of functionality- induced locking of ZIF-78-Co at the MS beamline of the SESAME synchrotron (Figure S3.7 in SI).

2.3. Gas Adsorption. Ultrahigh-grade gases (99.999%) such as He, N_2, CO_2, and CH_4 were used throughout the experiments. A liquid nitrogen bath was used for the temperatures controlled at 77 and 112 K with a CryoSync from Quantachrome; a dry ice/methanol
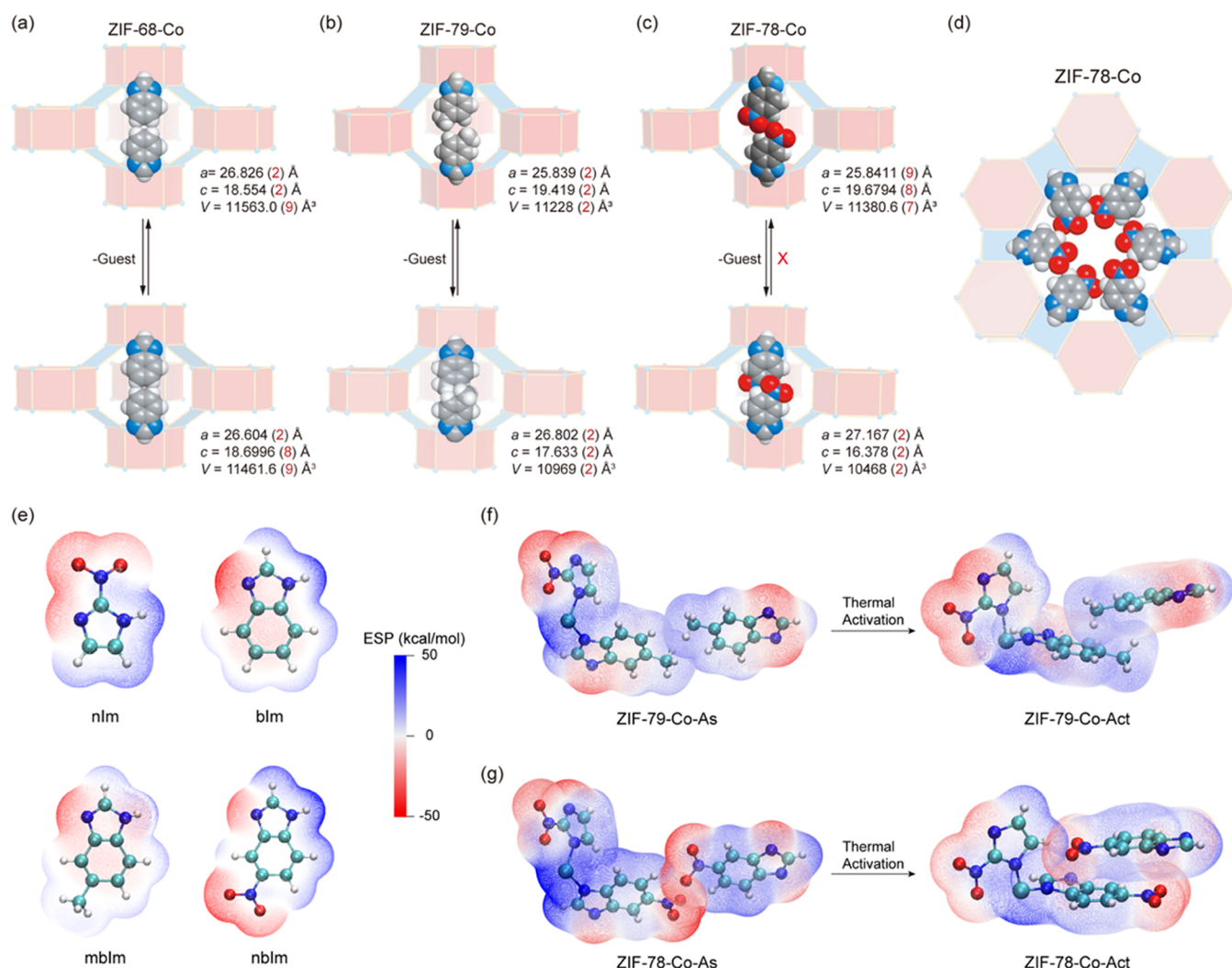
Figure 2. Structural transformations of the dynamic ZIFs upon guest removal as characterized by SCXRD and PXRD analyses. Illustration of the dynamic locking mechanism observed for the frameworks by linker−linker interactions in (a) ZIF-68-Co, (b) ZIF-79-Co, and (c) ZIF-78-Co through van der Waals interaction, C−H⋯π interaction, and π⋯π stacking, respectively. (d) Top view along the c axis of activated ZIF-78-Co. Electrostatic potential (ESP)-colored van der Waals surface maps of (e) imidazole organic linkers used in this work; (f) truncated segment of ZIF-79-Co; and (g) truncated segment ZIF-78-Co. ESP is colored according to the color bar on the system's van der Waals surface (ρ = 0.001 a.u.).

bath was used for the temperature held at 195 K; a recirculating Dewar connected to a Julabo F25-ME isothermal bath was used for controlling temperatures at 273, 283, 298, and 308 K. Low-pressure gas/vapor adsorption isotherms were measured volumetrically using a Quantachrome iQ (N_2, CO_2, and CH_4) or Microtac BELsorp Max2 (n-C_4H_{10}, CH_3OH, and H_2O) sorption analyzer. High-pressure adsorption isotherms (0−30 bar) were measured on a Quantachrome iSorb HP1 instrument. High-pressure dynamic adsorption break-through curves were evaluated using a Hiden ABR automated breakthrough analyzer (Sections S4−S8 in SI).

2.4. Electrostatic Potential (ESP)-Colored van der Waals Surface Maps. The ESP-colored van der Waals surface maps of ZIFs were evaluated based on the effective algorithm proposed by Multiwfn (Section S9 in SI).[53,54] The segments used to illustrate the distinct interactions were clipped from the structures of ZIFs obtained from single-crystal X-ray diffraction (SCXRD) data.

3. RESULTS AND DISCUSSION

3.1. Identification of Functionality-Induced Locking of ZIFs. The functionality-induced locking of ZIFs was initially identified by comparing PXRD patterns of as-synthesized, activated, and re-solvated samples (Figure 1a−c). Without

functionalization, the PXRD patterns for as-synthesized and activated ZIF-68-Co exhibit similar diffraction peak positions with changes only in their intensity, indicating the constant framework geometry upon activation (Figure 1a). Contrast-ingly, the PXRD patterns for as-synthesized and activated ZIF-79-Co show distinct diffraction peak positions with the 100 reflection shifted to a lower 2θ angle and the 101 and 110 reflections shifted to higher 2θ angles, thereby revealing a significant structural transformation upon thermal activation (Figure 1b). The PXRD patterns of the re-solvated ZIF-79-Co were recovered only after being immersed in DMF, which suggested a reversible flexibility of the framework. A similar structural transformation was also observed in the PXRD pattern comparison for the as-synthesized and activated ZIF-78-Co, showing the 100 and 101 peak positions shifting from 3.95 to 3.82° and 5.98 to 6.69°, respectively (Figure 1c). Strikingly, the PXRD pattern of re-solvated ZIF-78-Co retains the peak positions similar to its activated one, indicating irreversible structural transformation.

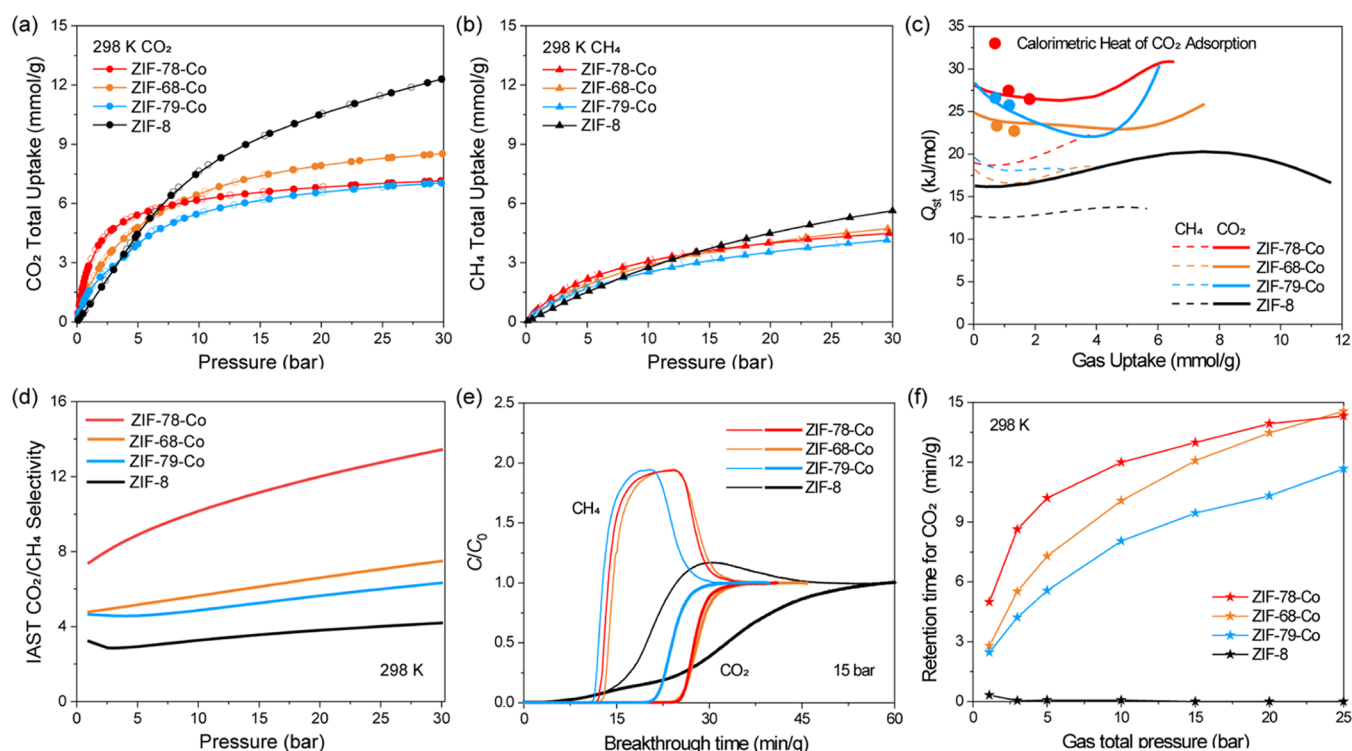The N_2 adsorption isotherms at 77 K show shrinkage of pore sizes and pore volumes after functionalization (Figure 1d−e)

Figure 3. Evaluation of CO_2/CH_4 adsorptive separation performance via high-pressure gas uptake isotherms and dynamic breakthrough measurements. High-pressure total gas uptake isotherms at 298 K for ZIF-68-Co (orange), −78-Co (red), −79-Co (blue), and ZIF-8 (black) for (a) CO_2 and (b) CH_4. (c) Heats of CH_4 and CO_2 adsorption were measured from a thermogravimetric analyzer coupled to a differential scanning calorimeter (TG-DSC) and calculated from their high-pressure adsorption isotherms for several temperatures using virial model fitting (solid line). (d) Pressure-dependent CO_2/CH_4 selectivity based on the IAST model. (e) Dynamic adsorption breakthrough curves for the GME-ZIFs at 298 K and 15 bar with a 1:1 (v/v) ratio of CH_4 and CO_2 and a 5 mL/min flow rate. (f) Retention time of CO_2 calculated from CO_2/CH_4 breakthrough curves (CO_2/CH_4 = 50:50) at 298 K.

since the bulkiness of the functional groups increased gradually for ZIF-68-Co, ZIF-79-Co, and ZIF-78-Co. The pore size distributions of the three ZIFs derived from their N_2 adsorption isotherms were 10.1/7.2, 8.2, and 6.7 Å, respectively (inset in Figure 1d). The pore volumes calculated from the N_2 uptakes at $P/P_0 \sim 0.99$ for ZIF-68-Co, ZIF-79-Co, and ZIF-78-Co were 0.49, 0.40, and 0.30 $cm^3\ g^{-1}$, respectively. Similar pore volumes were obtained from the saturated adsorption capacity of CH_4 and CO_2 (Figure 1e,f). These results are consistent with the calculated pore volumes (Table S4.1 in SI), suggesting the accessibility of all cavities upon functionalization. The step-wise CO_2 adsorption for ZIF-68-Co behaviors can be attributed to the bi-porous systems, which have been validated by molecular simulation using the grand canonical Monte Carlo (GCMC) method (Figures S4.1−S4.3 in SI).

It is noted that when adsorbing guest molecules at room temperature, the difference in dynamic behaviors appeared, which was related to the polarity of the guest molecules.[55] While adsorbing nonpolar *n*-butane, all three ZIFs showed type I adsorption isotherms, with changes only in their adsorption amount (Figure 1g). Owing to the bulky *n*-butane molecule, the calculated pore volume is lower than the theoretical value, consistent with methanol (CH_3OH) adsorption results. While adsorbing polar CH_3OH, ZIF-68-Co exhibited two-step adsorption behavior without apparent hysteresis, which may be ascribed to the swinging motions of the linkers without functional groups (Figure 1h). This was in contrast to the remarkable dynamic behavior observed in ZIF-79-Co. For this

compound, a significant two-step adsorption process was followed with a non-negligible hysteresis loop, suggesting that a structural transition may occur during the adsorption process. Due to functionality-induced locking of the framework, ZIF-78-Co exhibited one-step adsorption isotherms for CH_3OH adsorption. H_2O adsorption at 298 K showed that functionalization could change the hydrophilicity of the material, in which the nitro-functionalized ZIF-78-Co was hydrophilic, while the unfunctionalized ZIF-68-Co and the methyl-functionalized ZIF-79-Co were relatively hydrophobic (Figure 1i).

3.2. Molecular Insight into Functionality-Induced Locking of ZIFs. The SCXRD results of the GME variants helped us to understand the dynamic structural transformation at the atomic level (Figure 2). The results showed that they were all isostructural and crystallized in the space group $P6_3/mmc$ (no. 194). Each tetrahedral Co^{II} ion is connected to two nIm and two functionalized bIm, linked together via angular sharing to form a three-dimensional framework of GME topology. Due to the structural contraction, the activated structures of ZIF-78-Co and ZIF-79-Co were refined in the lower symmetry space group $P6_3$ (no. 173) to handle the substantial disorder. For ZIF-68-Co with nonfunctionalized bIm, only slight changes to the unit cell parameters were observed, in which the value of *a* parameter decreased from 26.826(2) to 26.604(2) Å, while the *c* parameter increased from 18.554(2) to 18.6696(8) Å (Figure 2a), indicating that its framework geometry remained constant upon activation. Furthermore, only weaker van der Waals interactions were

observed between two adjacent bIms, as confirmed by the ESP maps of the as-synthesized and activated ZIF-68-Co (Figure S9.1 in SI). On the contrary, for ZIF-79-Co with methyl-functionalized bIm, the structure contracted by 2.31% in cell volume, in which the cell parameter in the a direction increased from 25.839(2) to 26.802(2) Å, while the c parameter reduced from 19.419(2) to 17.633(2) Å (Figure 2b). The ESP maps of as-synthesized and activated ZIF-79-Co illustrated a C−H⋯π interaction between two mbIm. The relatively weak interaction cannot lock the framework, leading to a reversible structural transformation (Figure 2f). Notice-ably, for ZIF-78-Co, with nitro-functionalized bIm, a significant structural contraction occurred (up to 8.02% reduction in cell volume) upon thermal activation, in which the length of the a-axis increased from 25.8411(9) to 27.167(2) Å, while the length of the c-axis reduced from 19.6794(8) to 16.378(2) Å (Figure 2c). The top view along the c-axis of activated ZIF-78-Co illustrated that the 12-ring was formed by the alternating coordination of nIm and nbIm (Figure 2d). By comparing the ESP maps of as-synthesized and activated ZIF-78-Co, it was found that in addition to the strong π⋯π interaction between two nbIm, an extra strong intermolecular hydrogen bonding to the adjacent nIm was also observed (Figure 2g). These interactions synergistically lock the structure and render the framework transformation irreversible.

3.3. Adsorptive Separation Performance upon Functionality-Induced Locking.
High-pressure (0−30 bar) CO_2 and CH_4 gas adsorption isotherms were measured for the GME-ZIFs at 273, 298, and 308 K (Figures S5.1−S5.6 in SI). As shown in Figure 3a,b, all ZIFs exhibited higher affinity and capacity for CO_2 over CH_4. The CO_2 uptake for ZIF-68-Co, −79-Co −78-Co, and −8 at 298 K and 5 bar was 4.8, 3.9, 5.5, and 4.5 mmol/g, respectively, which was 2- to 3-fold higher than that of CH_4. Consequently, CH_4 and CO_2 adsorption heats of adsorption, calculated from high-pressure adsorption isotherms at several temperatures and fitted with the virial model, suggested stronger interactions between the framework and CO_2 (Figure 3c). When 1 mmol/g of gas was adsorbed, CO_2 adsorption heat for ZIF-68-Co, −79-Co, −78-Co, and −8 was 23.8, 25.4, 26.9, and 16.2 kJ/mol, respectively, while CH_4 adsorption heat was 16.6, 18.1, 18.7, and 12.6 kJ/mol, respectively. The calorimetric adsorption heats measured from the TG-DSC test were consistent with the simulated results, in which CH_4 has no accurate adsorption heat due to its low adsorption capacity (Figures S6.7−S6.12 in SI). Using the CO_2 and CH_4 adsorption isotherm data, ideal adsorbed solution theory (IAST) was applied to estimate the selectivity of the framework toward CO_2 over CH_4 (Figure 3d). Specifically, for an equimolar mixture of CO_2 and CH_4 at 298 K and 3000 kPa, the adsorption selectivities of ZIF-68-Co, ZIF-79-Co, and ZIF-78-Co were 7.1, 5.9, and 12.8, respectively, which surpassed that of ZIF-8 (3.9) and were comparable with values calculated for several state-of-the-art MOFs for CO_2/CH_4 separation (Table S7.1 in SI).

The activated samples of the three GME-ZIFs were then shown to achieve excellent separation performances via dynamic breakthrough experiments of CO_2/CH_4 compared to ZIF-8, which were consistent with the results of high-pressure gas adsorption measurements. As shown in Figure 3e, a highly efficient separation of the CO_2/CH_4 mixture was achieved by each selected ZIF. As predicted, CH_4 was the first gas to elute through the adsorption bed with a high-purity grade of 99.1%, reaching saturation rapidly. At the same time,

CO_2 was retained for a significant amount of time, equal to 12.1, 9.4, and 13.1 min/g for ZIF-68-Co, −79-Co, and −78-Co, respectively (Figure 3f). Compared with the GME-ZIFs synthesized in this work, the flexible ZIF-8 displayed an ineffective separation capability. Specifically, from the break-through curves, CH_4 at high purity was obtained for extended periods when the three GME-ZIFs were compared to ZIF-8; a compound that showed difficulty in purifying CH_4 under the same conditions. Strikingly, ZIF-78-Co, with nitro-function-alized bIm, exhibited the best separation performance among these ZIFs, as highlighted by the longest retention time for CO_2 and, therefore, the highest CH_4 purified amount. In the competitive dynamic adsorption process, ZIF-78-Co adsorbed slightly less CO_2 than the amount calculated from the single-component dynamic adsorption curve (Figure S8.7 in SI), while the amount of CH_4 adsorbed dropped significantly, leading to a much higher dynamic selectivity as compared to the theoretical IAST selectivity.

The findings herein highlight the importance of deliberate control over framework dynamics by functionalization and precise regulation of a ZIF's inherent flexibility by function-ality-induced linker locking to improve gas separation under experimental conditions.[56−61] In addition, low energy con-sumption and time efficiency throughout the regeneration and recycling processes are highly significant in industrial settings. For the case of each GME-ZIF, regeneration was fully realized under mild conditions by simply purging the ZIF-containing bed with Ar without changing the temperature conditions.

4. CONCLUSIONS
By targeting framework flexibility through molecular design, one reported and two new GME-ZIFs were prepared and studied in this work. The effects of functionalization on structural flexibility and gas separation were systematically investigated by combining XRD analyses, gas adsorption, and dynamic breakthrough experiments. The functionality-induced locking uncovered here fundamentally differs from the linker swing dynamics[16−19] and flexible deformation[21] previously observed in ZIFs. A rigid porous structure maximizes the linker−linker interaction through irreversible structural trans-formation upon thermal treatment. Such functionality-induced locking influenced the structural change experienced by the respective GME-ZIFs and their practical performance in high-pressure gas adsorptive separation. Among the reported GME-ZIFs, ZIF-78-Co, having the most rigid structure, achieved the best CO_2/CH_4 separation performance, thereby correlating a higher gas separation performance to the desired structural attributes of pore size, structure, and environment (i.e., functionalization). The overarching principle detailed in this work provides general guidance for molecular design when developing next-generation porous adsorbents.

■ ASSOCIATED CONTENT

ⓢ Supporting Information
The Supporting Information is available free of charge at https://pubs.acs.org/doi/10.1021/acs.chemmater.2c02832.

> Synthetic procedure, PXRD patterns, NMR and IR spectra, SEM pictures, TGA curves, SCXRD results, gas sorption isotherms, dynamic gas adsorption break-through curves, and ESP-colored van der Waals surface maps (PDF)

> ZIF-68-Co (CIF)

ZIF-68-Co-activated (CIF)
ZIF-78-Co (CIF)
ZIF-78-Co-activated (CIF)
ZIF-79-Co (CIF)
ZIF-79-Co-activated (CIF)

■ AUTHOR INFORMATION

Corresponding Author

Yue-Biao Zhang − *Shanghai Key Laboratory of High-Resolution Electron Microscopy, School of Physical Science and Technology, ShanghaiTech University, Shanghai 201210, China;* ● orcid.org/0000-0002-8270-1067; Email: zhangyb@shanghaitech.edu.cn

Authors

Tongtong Xu − *Shanghai Key Laboratory of High-Resolution Electron Microscopy, School of Physical Science and Technology, ShanghaiTech University, Shanghai 201210, China*

Beibei Zhou − *Shanghai Key Laboratory of High-Resolution Electron Microscopy, School of Physical Science and Technology, ShanghaiTech University, Shanghai 201210, China*

Yu Tao − *Shanghai Key Laboratory of High-Resolution Electron Microscopy, School of Physical Science and Technology, ShanghaiTech University, Shanghai 201210, China*

Zhaolin Shi − *Shanghai Key Laboratory of High-Resolution Electron Microscopy, School of Physical Science and Technology, ShanghaiTech University, Shanghai 201210, China;* ● orcid.org/0000-0001-9698-4152

Wentao Jiang − *Shanghai Key Laboratory of High-Resolution Electron Microscopy, School of Physical Science and Technology, ShanghaiTech University, Shanghai 201210, China;* ● orcid.org/0000-0002-5376-3381

Mahmoud Abdellatief − *Synchrotron-Light for Experimental Science and Applications in the Middle East (SESAME), Allan 19252, Jordan*

Kyle E. Cordova − *Materials Discovery Research Unit, Advanced Research Center, Royal Scientific Society, Amman 11941, Jordan;* ● orcid.org/0000-0002-4988-0497

Complete contact information is available at:
https://pubs.acs.org/10.1021/acs.chemmater.2c02832

Notes

The authors declare no competing financial interest.

■ REFERENCES

(1) Furukawa, H.; Cordova, K. E.; O'Keeffe, M.; Yaghi, O. M. The Chemistry and Applications of Metal-Organic Frameworks. *Science* **2013**, *341*, No. 1230444.

(2) Yaghi, O. M.; Kalmutzki, M. J.; Diercks, C. S. *Introduction to Reticular Chemistry: Metal−Organic Frameworks and Covalent Organic Frameworks*; Wiley-VCH: Weinheim, Germany, 2019; pp 463−479.

(3) Tian, Y. Q.; Cai, C. X.; Ji, Y.; You, X. Z.; Peng, S. M.; Lee, G. H. $[Co_5(im)_{10}\cdot 2MB]_\infty$: A Metal-Organic Open-Framework with Zeolite-Like Topology. *Angew. Chem., Int. Ed.* **2002**, *114*, 1442−1444.

(4) Huang, X. C.; Lin, Y. Y.; Zhang, J. P.; Chen, X. M. Ligand-Directed Strategy for Zeolite-Type Metal-Organic Frameworks: Zinc(II) Imidazolates with Unusual Zeolitic Topologies. *Angew. Chem., Int. Ed.* **2006**, *45*, 1557−1559.

(5) Park, K. S.; Ni, Z.; Côté, A. P.; Choi, J. Y.; Huang, R. D.; Uribe-Romo, F. J.; Chae, H. K.; O'Keeffe, M.; Yaghi, O. M. Exceptional Chemical and Thermal Stability of Zeolitic Imidazolate Frameworks. *Proc. Natl. Acad. Sci. U.S.A.* **2006**, *103*, 10186−10191.

(6) Tian, Y. Q.; Cai, C. X.; Ren, X. M.; Duan, C. Y.; Xu, Y.; Gao, S.; You, X. Z. The Silica-Like Extended Polymorphism of Cobalt(II) Imidazolate Three-Dimensional Frameworks: X-ray Single-Crystal Structures and Magnetic Properties. *Chem. Eur. J.* **2003**, *9*, 5673−5685.

(7) Zhang, J.; Wu, T.; Zhou, C.; Chen, S.; Feng, P.; Bu, X. Zeolitic Boron Imidazolate Frameworks. *Angew. Chem., Int. Ed.* **2009**, *48*, 2542−2545.

(8) Phan, A.; Doonan, C. J.; Uribe-Romo, F. J.; Knobler, C. B.; O'Keeffe, M.; Yaghi, O. M. Synthesis, Structure, and Carbon Dioxide Capture Properties of Zeolitic Imidazolate Frameworks. *Acc. Chem. Res.* **2010**, *43*, 58−67.

(9) Zhang, J. P.; Zhang, Y. B.; Lin, J. B.; Chen, X. M. Metal Azolate Frameworks: from Crystal Engineering to Functional Materials. *Chem. Rev.* **2012**, *112*, 1001−1033.

(10) Noh, K.; Lee, J.; Kim, J. Compositions and Structures of Zeolitic Imidazolate Frameworks. *Isr. J. Chem.* **2018**, *58*, 9−10.

(11) Tan, Y. X.; Wang, F.; Zhang, J. Design and Synthesis of Multifunctional Metal-Organic Zeolites. *Chem. Soc. Rev.* **2018**, *47*, 2130−2144.

(12) Wang, H. Z.; Pei, X. K.; Kalmutzki, M. J.; Yang, J. J.; Yaghi, O. M. Large Cages of Zeolitic Imidazolate Frameworks. *Acc. Chem. Res.* **2022**, *55*, 707−721.

(13) Banerjee, R.; Phan, A.; Wang, B.; Knobler, C.; Furukawa, H.; O'Keeffe, M.; Yaghi, O. M. High-Throughput Synthesis of Zeolitic Imidazolate Frameworks and Application to CO_2 Capture. *Science* **2008**, *319*, 939−943.

(14) Peng, Y.; Li, Y. S.; Ban, Y. J.; Jin, H.; Jiao, W. M.; Liu, X. L.; Yang, W. S. Metal-Organic Framework Nanosheets as Building Blocks for Molecular Sieving Membranes. *Science* **2014**, *346*, 1356−1359.

(15) Ma, X. L.; Kumar, P.; Mittal, N.; Khlyustova, A.; Daoutidis, P.; Mkhoyan, K. A.; Tsapatsis, M. Zeolitic Imidazolate Framework Membranes Made by Ligand-Induced Permselectivity. *Science.* **2018**, *361*, 1008−1011.

(16) Fairen-Jimenez, D.; Moggach, S. A.; Wharmby, M. T.; Wright, P. A.; Parsons, S.; Düren, T. Opening the Gate: Framework Flexibility in ZIF-8 Explored by Experiments and Simulations. *J. Am. Chem. Soc.* **2011**, *133*, 8900−8902.

(17) Zhang, J. P.; Zhu, A. X.; Chen, X. M. Single-crystal X-ray Diffraction and Raman Spectroscopy Studies of Isobaric N_2 Adsorption in SOD-type Metal−Organic Zeolites. *Chem. Commun.* **2012**, *48*, 11395−11397.

(18) Ania, C. O.; García-Pérez, E.; Haro, M.; Gutiérrez-Sevillano, J. J.; Valdés-Solís, T.; Parra, J. B.; Calero, S. Understanding Gas-Induced Structural Deformation of ZIF-8. *J. Phys. Chem. Lett.* **2012**, *3*, 1159−64.

(19) Zhang, L.; Hu, Z.; Jiang, J. Sorption-Induced Structural Transition of Zeolitic Imidazolate Framework-8: A Hybrid Molecular Simulation Study. *J. Am. Chem. Soc.* **2013**, *135*, 3722−3728.

(20) Choi, Y.; Noh, K.; Lee, J.; Kim, J. Porosity Properties of the Conformers of Sodalite-like Zeolitic Imidazolate Frameworks. *J. Am. Chem. Soc.* **2018**, *140*, 14586−14589.

(21) Gao, M.; Huang, R.-K.; Zheng, B.; Wang, P.; Shi, Q.; Zhang, W.-X.; Dong, J. Large Breathing Effect in ZIF-65(Zn) with Expansion and Contraction of the SOD cage. *Nat. Commun.* **2022**, *13*, No. 4569.

(22) Horike, S.; Shimomura, S.; Kitagawa, S. Soft Porous Crystals. *Nat. Chem.* **2009**, *1*, 695−704.

(23) Pimentel, B. R.; Parulkar, A.; Zhou, E.; Brunelli, N. A.; Lively, R. P. Zeolitic Imidazolate Frameworks: Next-Generation Materials for Energy-Efficient Gas Separations. *ChemSusChem* **2014**, *7*, 3202−3240.

(24) Schneemann, A.; Bon, V.; Schwedler, I.; Senkovska, I.; Kaskel, S.; Fischer, R. A. Flexible Metal−Organic Frameworks. *Chem. Soc. Rev.* **2014**, *43*, 6062−6096.

(25) Coudert, F.-X.; Evans, J. D. Nanoscale Metamaterials: Meta-MOFs and Framework Materials with Anomalous Behavior. *Coord. Chem. Rev.* **2019**, *388*, 48−62.

(26) Iacomi, P.; Maurin, G. ResponZIF Structures: Zeolitic Imidazolate Frameworks as Stimuli-Responsive Materials. *ACS Appl. Mater. Interfaces* **2021**, *13*, 50602−50642.

(27) Knebel, A.; Geppert, B.; Volgmann, K.; Kolokolov, D. I.; Stepanov, A. G.; Twiefel, J.; Heitjans, P.; Volkmer, D.; Caro, J. Defibrillation of Soft Porous Metal−Organic Frameworks with Electric Fields. *Science* **2017**, *358*, 347−351.

(28) Gao, H. Q.; Wei, W. J.; Dong, L. Y.; Feng, G. Q.; Jiang, X. X.; Wu, R.; Lin, Z. S.; Li, W. Enhanced Framework Rigidity of a Zeolitic Metal-Azolate via Ligand Substitution. *Crystals* **2017**, *7*, No. 99.

(29) Zhou, S.; Wei, Y. Y.; Li, L. B.; Duan, Y. F.; Hou, Q. Q.; Zhang, L. L.; Ding, L. X.; Xue, J.; Wang, H. H.; Caro, J. Paralyzed Membrane: Current-driven Synthesis of a Metal-organic Framework with Sharpened Propene/Propane Separation. *Sci. Adv.* **2018**, *4*, No. eaau1393.

(30) Xiang, L.; Liu, D. H.; Jin, H.; Xu, L.-W.; Wang, C. Q.; Xu, S. T.; Pan, Y. C.; Li, Y. S. Locking of Phase Transition in MOF ZIF-7: Improved Selectivity in Mixed-matrix Membranes for O_2/N_2 Separation. *Mater. Horiz.* **2020**, *7*, 223−228.

(31) Zhang, J. P.; Zhou, H. L.; Zhou, D. D.; Liao, P. Q.; Chen, X. M. Controlling Flexibility of Metal−Organic Frameworks. *Natl. Sci. Rev.* **2018**, *5*, 907−919.

(32) McGuirk, C. M.; Runčevski, T.; Oktawiec, J.; Turkiewicz, A.; Taylor, M. K.; Long, J. R. Influence of Metal Substitution on the Pressure-Induced Phase Change in Flexible Zeolitic Imidazolate Frameworks. *J. Am. Chem. Soc.* **2018**, *140*, 15924−15933.

(33) Zhang, X. W.; Zhou, D. D.; Zhang, J. P. Tuning the Gating Energy Barrier of Metalorganic Framework for Molecular Sieving. *Chem.* **2021**, *7*, 1006−1019.

(34) Wang, B.; Côté, A. P.; Furukawa, H.; O'Keeffe, M.; Yaghi, O. M. Colossal Cages in Zeolitic Imidazolate Frameworks as Selective Carbon Dioxide Reservoirs. *Nature* **2008**, *453*, 207−211.

(35) Wu, T.; Bu, X. H.; Liu, R.; Lin, Z. E.; Zhang, J.; Feng, P. Y. A New Zeolitic Topology with Sixteen-Membered Ring and Multi-dimensional Large Pore Channels. *Chem. Eur. J.* **2008**, *14*, 7771−7773.

(36) Lyndon, R.; You, W. Q.; Ma, Y.; Basca, J.; Gong, Y. T.; Stangland, E. E.; Walton, K. S.; Sholl, D. S.; Lively, R. P. Tuning the Structures of Metal−Organic Frameworks via a Mixed-Linker Strategy

for Ethylene/Ethane Kinetic Separation. *Chem. Mater.* **2020**, *32*, 3715−3722.

(37) Zha, X. Y.; Li, X. H.; Al-Omari, A. A.; Liu, S.; Liang, C. C.; Al-Ghourani, A.; Abdellatief, M.; Yang, J. J.; Nguyen, H. L.; Al-Maythalony, B.; Shi, Z. L.; Cordova, K. E.; Zhang, Y. B. Zeolite NPO-Type Azolate Frameworks. *Angew. Chem. Int. Ed.* **2022**, *61*, No. e202207467.

(38) Hayashi, H.; Côté, A. P.; Furukawa, H.; O'Keeffe, M.; Yaghi, O. M. Zeolite A Imidazolate Frameworks. *Nat. Mater.* **2007**, *6*, 501−506.

(39) Wu, T.; Bu, X.; Zhang, J.; Feng, P. New Zeolitic Imidazolate Frameworks: From Unprecedented Assembly of Cubic Clusters to Ordered Cooperative Organization of Complementary Ligands. *Chem. Mater.* **2008**, *20*, 7377−7382.

(40) Nguyen, N. T. T.; Furukawa, H.; Gándara, F.; Nguyen, H. T.; Cordova, K. E.; Yaghi, O. M. Selective Capture of Carbon Dioxide under Humid Conditions by Hydrophobic Chabazite-Type Zeolitic Imidazolate Frameworks. *Angew. Chem., Int. Ed.* **2014**, *53*, 10645−10648.

(41) Yang, J. J.; Zhang, Y. B.; Liu, Q.; Trickett, C. A.; Gutiérrez-Puebla, E.; Monge, M. A.; Cong, H. J.; Aldossary, A.; Deng, H. X.; Yaghi, O. M. Principles of Designing Extra-Large Pore Openings and Cages in Zeolitic Imidazolate Frameworks. *J. Am. Chem. Soc.* **2017**, *139*, 6448−6455.

(42) Banerjee, R.; Furukawa, H.; Britt, D.; Knobler, C.; O'Keeffe, M.; Yaghi, O. M. Control of Pore Size and Functionality in Isoreticular Zeolitic Imidazolate Frameworks and their Carbon Dioxide Selective Capture Properties. *J. Am. Chem. Soc.* **2009**, *131*, 3875−3877.

(43) Cho, H. S.; Yang, J.; Gong, X.; Zhang, Y. B.; Momma, K.; Weckhuysen, B. M.; Deng, H.; Kang, J. K.; Yaghi, O. M.; Terasaki, O. Isotherms of Individual Pores by Gas Adsorption Crystallography. *Nat. Chem.* **2019**, *11*, 562−570.

(44) Sudik, A. C.; Ockwig, N. W.; Côté, A. P.; Yaghi, O. M. Metal-Organic Frameworks Based on Trigonal Prismatic Building Blocks and the New "**acs**" Topology. *Inorg. Chem.* **2005**, *44*, 2998−3000.

(45) Serre, C.; Mellot-Draznieks, C.; Surblé, S.; Audebrand, N.; Filinchuk, Y.; Férey, G. Role of Solvent-Host Interactions that Lead to Very Large Swelling of Hybrid Frameworks. *Science* **2007**, *315*, 1828−1831.

(46) Mellot-Draznieks, C.; Serre, C.; Surblé, S.; Audebrand, N.; Férey, G. Very Large Swelling in Hybrid Frameworks: A Combined Computational and Powder Diffraction Study. *J. Am. Chem. Soc.* **2005**, *127*, 16273−16278.

(47) Zhou, B. B.; Zeng, T. W.; Shi, Z. L.; Zhang, G.; Horike, S.; Zhang, Y.-B. An Allosteric Metal-Organic Framework Exhibits Multiple Pore Configurations for the Optimization of Hydrocarbon Separation. *Chem. Asian J.* **2019**, *14*, 3552−3556.

(48) Tan, J.; Tao, Y.; Zhang, X. Y.; Wang, Q.; Zeng, T. W.; Shi, Z. L.; Cordova, K. E.; Lee, Y.; Liu, H. M.; Zhang, Y.-B. Control over Interpenetration for Boosting Methane Storage Capacity in Metal-Organic Frameworks. *J. Mater. Chem. A* **2021**, *9*, 24857−24862.

(49) Ma, Y.-X.; Li, Z.-J.; Wei, L.; Ding, S.-Y.; Zhang, Y.-B.; Wang, W. A Dynamic Three-Dimensional Covalent Organic Framework. *J. Am. Chem. Soc.* **2017**, *139*, 4995−4998.

(50) Chen, Y. C.; Shi, Z. L.; Wei, L.; Zhou, B. B.; Tan, J.; Zhou, H.-L.; Zhang, Y.-B. Guest-Dependent Dynamics in a 3D Covalent Organic Framework. *J. Am. Chem. Soc.* **2019**, *141*, 3298−3303.

(51) Ma, T. Q.; Wei, L.; Liang, L.; Yin, S.; Xu, L.; Niu, J.; Xue, H.; Wang, X.; Sun, J.; Zhang, Y.-B.; Wang, W. Diverse Crystal Size Effects in Covalent Organic Frameworks. *Nat. Commun.* **2020**, *11*, No. 6128.

(52) Panda, T.; Gupta, K. M.; Jiang, J.-W.; Banerjee, R. Enhancement of CO_2 Uptake in Iso-reticular Co Based Zeolitic Imidazolate Frameworks via Metal Replacement. *CrystEngComm* **2014**, *16*, 4677−4680.

(53) Zhang, J.; Lu, T. Efficient Evaluation of Electrostatic Potential with Computerized Optimized Code. *Phys. Chem. Chem. Phys.* **2021**, *23*, 20323−20328.

(54) Lu, T.; Chen, F. Multiwfn: A Multifunctional Wavefunction Analyzer. *J. Comput. Chem.* **2012**, *33*, 580−92.

H

(55) Cho, H. S.; Tanaka, H.; Lee, Y.; Zhang, Y.-B.; Jiang, J.; Kim, M.; Kim, H.; Kang, J. K.; Terasaki, O. Physicochemical Understanding of the Impact of Pore Environment and Species of Adsorbates on Adsorption Behaviour. *Angew. Chem. Int. Ed.* **2021**, *60*, 20504−20510.

(56) Haszeldine, R. S. Carbon Capture, and Storage: How Green Can Black Be? *Science* **2009**, *325*, 1647−1652.

(57) Vitillo, J. G.; Smit, B.; Gagliardi, L. Introduction: Carbon Capture and Separation. *Chem. Rev.* **2017**, *117*, 9521−9523.

(58) Li, J.-R.; Sculley, J.; Zhou, H.-C. Metal−Organic Frameworks for Separations. *Chem. Rev.* **2012**, *112*, 869−932.

(59) Nugent, P.; Belmabkhout, Y.; Burd, S. D.; Cairns, A. J.; Luebke, R.; Forrest, K.; Pham, T.; Ma, S.; Space, B.; Wojtas, L.; Eddaoudi, M.; Zaworotko, M. Porous Materials with Optimal Adsorption Thermodynamics and Kinetics for CO_2 Separation. *Nature* **2013**, *495*, 80−84.

(60) Zhang, Z.; Yao, Z.-Z.; Xiang, S.; Chen, B. Perspective of Microporous Metal−Organic Frameworks for CO_2 Capture and Separation. *Energy Environ. Sci.* **2014**, *7*, 2868−2899.

(61) Yu, J.; Xie, L.-H.; Li, J.-R.; Ma, Y.; Seminario, J. M.; Balbuena, P. B. CO_2 Capture and Separations Using MOFs: Computational and Experimental Studies. *Chem. Rev.* **2017**, *117*, 9674−9754.